2011

Multispecies diffusion models: A study of uranyl species diffusion

Chongxuan Liu
Pacific Northwest National Laboratory, chongxuan.liu@pnl.gov

Jianying Shang
Pacific Northwest National Laboratory

John M. Zachara
Pacific Northwest National Laboratory, john.zachara@pnl.gov

Multispecies diffusion models: A study of uranyl species diffusion

Chongxuan Liu,[1] Jianying Shang,[1] and John M. Zachara[1]

Received 18 February 2011; revised 10 October 2011; accepted 22 October 2011; published 15 December 2011.

[1] Rigorous numerical description of multispecies diffusion requires coupling of species, charge, and aqueous and surface complexation reactions that collectively affect diffusive fluxes. The applicability of a fully coupled diffusion model is, however, often constrained by the availability of species self-diffusion coefficients, as well as by computational complication in imposing charge conservation. In this study, several diffusion models with variable complexity in charge and species coupling were formulated and compared to describe reactive multispecies diffusion in groundwater. Diffusion of uranyl [U(VI)] species was used as an example in demonstrating the effectiveness of the models in describing multispecies diffusion. Numerical simulations found that a diffusion model with a single, common diffusion coefficient for all species was sufficient to describe multispecies U(VI) diffusion under a steady state condition of major chemical composition, but not under transient chemical conditions. Simulations revealed that for multispecies U(VI) diffusion under transient chemical conditions, a fully coupled diffusion model could be well approximated by a component-based diffusion model when the diffusion coefficient for each chemical component was properly selected. The component-based diffusion model considers the difference in diffusion coefficients between chemical components, but not between the species within each chemical component. This treatment significantly enhanced computational efficiency at the expense of minor charge conservation. The charge balance in the component-based diffusion model can be enforced, if necessary, by adding a secondary migration term resulting from model simplification. The effect of ion activity coefficient gradients on multispecies diffusion is also discussed. The diffusion models were applied to describe U(VI) diffusive mass transfer in intragranular domains in two sediments collected from U.S. Department of Energy's Hanford 300A, where intragranular diffusion is a rate-limiting process controlling U(VI) adsorption and desorption. The grain-scale reactive diffusion model was able to describe U(VI) adsorption/desorption kinetics that had been previously described using a semiempirical, multirate model. Compared with the multirate model, the diffusion models have the advantage to provide spatiotemporal speciation evolution within the diffusion domains.

Citation: Liu, C., J. Shang, and J. M. Zachara (2011), Multispecies diffusion models: A study of uranyl species diffusion, *Water Resour. Res.*, *47*, W12514, doi:10.1029/2011WR010575.

1. Introduction

[2] Diffusion is an important process controlling grain-scale sorption and desorption kinetics [*Ball and Roberts*, 1991; *Cunningham et al.*, 1997; *Ewing et al.*, 2010; *Grathwohl*, 1998; *Miller and Pedit*, 1992; *Werth et al.*, 1997; *Wood et al.*, 1990], porescale reactive transport [*Kang et al.*, 2007; *Li et al.*, 2006, 2008; *Tartakovsky et al.*, 2007], and mass transfer in low-permeability zones and rock matrix [*Ball et al.*, 1997; *Brusseau*, 1991; *Liu and Ball*, 2002; *Parker et al.*, 2004; *Sawatsky et al.*, 1997; *Steefel and Litchner*, 1994; *Tokunaga et al.*, 2001; *Tokunaga et al.*, 2004] in subsurface environments. Diffusion of a multispecies contaminant, such as uranyl [U(VI)], is affected in complex ways by various factors including aqueous/surface speciation and solution chemical composition [*Felmy and Weare*, 1991; *Lasaga*, 1981; *Miller*, 1967a; *Van Cappellen and Gaillard*, 1996], and species and mineral surface charges and electrostatic potential [*Appelo and Wersin*, 2007; *Hart et al.*, 2001; *Liu et al.*, 2004; *Liu*, 2007; *Malusis and Shackelford*, 2002; *Nomura and Sakata*, 2001]. Rigorous numerical description of multispecies diffusion requires the full coupling of species, charge, aqueous, and surface complexation reactions that collectively affect species diffusive fluxes.

[3] Diffusion has been identified as a major mechanism controlling uranyl adsorption/desorption and precipitation/dissolution kinetics that was rate-limited by mass exchange to and from intragranular uranyl adsorption and precipitation locations [*McKinley et al.*, 2006; *Stubbs et al.*, 2009]. Diffusion also retarded U(VI) reactive transport in low permeable materials [*Bai et al.*, 2009; *Liu et al.*, 2010; *Yamaguchi et al.*, 1997; *Yamaguchi and Nakayama*, 1998] and in porous media containing mass transfer-limited domains [*Liu et al.*, 2008]. A fully species- and charge-coupled

[1]Pacific Northwest National Laboratory, Richland, Washington, USA.

model that integrates molecular speciation, charge, and geochemical reactions has been developed [e.g., *Appelo and Wersin*, 2007; *Giambalvo et al.*, 2002; *Lichtner*, 1996] that can be used to describe multispecies U(VI) diffusion in porous media [*Liu et al.*, 2006]. The applicability of the fully coupled multispecies diffusion model is, however, often constrained by the availability of self-diffusion coefficients as well as by computational complication in imposing local charge conservation. Consequently, modeling multispecies diffusion often assumes that all diffusing species have the same self-diffusion coefficient. The advantage of this simplification is that it guarantees local charge balance [*Van Cappellen and Gaillard*, 1996] and avoids complicated charge-separation and -induced electrostatic interaction [*Mafe et al.*, 1986]. This can significantly simplify numerical execution of the diffusion model, allowing development of porescale simulation approaches, such as lattice Boltzmann [*Kang et al.*, 2007; *Sukop and Thorne*, 2005] and smooth particle hydrodynamics [*Tartakovsky et al.*, 2007] for porescale simulations of diffusion-involved processes. The disadvantage of the approach is that it lacks theoretical rigor by ignoring species-specific diffusivity that may be important for the diffusion of multiple species with variable molecular size, charge, and hydration energy.

[4] In this study, we systematically compared four diffusion models with a variable degree of simplification in handling charge and species coupling in modeling multispecies diffusion. The models were compared for scenarios of U(VI) diffusion under both steady state and transient conditions of geochemical composition. The effect of an ionic activity coefficient gradient was also evaluated under a transient chemical condition with variable ionic strength. Species-specific self-diffusion coefficients recently estimated for U(VI) species from molecular calculations [*Kerisit and Liu*, 2010] were incorporated in a fully species- and charge-coupled model, which was used as a basis for comparing other diffusion models. The models were also applied and evaluated to describe experimental results of diffusion-limited intragranular U(VI) surface complexation reactions in a stirred flow-cell reactor. One of the major goals of this study was to identify the simplest model in numerical implementation that can provide sufficient accuracy to describe U(VI) reactive diffusion. The results also provided insights into the diffusion-limited U(VI) adsorption and desorption process in the intragranular and intergrain pore regions that were previously modeled using empirically based multirate or multidomain models [*Liu et al.*, 2009; *Qafoku et al.*, 2005].

2. Diffusion Models

[5] Multispecies diffusive fluxes may be described using the Nernst-Planck equation [*Bard and Faulkner*, 2001]:

$$J_i = -D_i \nabla c_i - \frac{Z_i F}{RT} D_i c_i \nabla \Psi, \; i = 1, 2, \ldots, N_s, \tag{1}$$

where J_i is the diffusive flux, c_i is the concentration, D_i is the self-diffusion coefficient, and Z_i is the charge of species i, respectively. F is the Faraday constant, R is the gas constant, T is the temperature, Ψ is the electrical potential, ∇ is the gradient symbol, and N_s is the number of species. Multiplying Z_i to equation (1) and summing equation (1) for all species yields the following electrical current equation induced by charged-species diffusion:

$$J_\sigma = F \sum_{i=1}^{N_s} Z_i J_i = -F \sum_{i=1}^{N_s} Z_i D_i \nabla c_i - F \frac{F}{RT} \sum_{i=1}^{N_s} Z_i^2 D_i c_i \nabla \Psi. \tag{2}$$

When the electrical current is zero ($J_\sigma = 0$), as in most cases in groundwater, the electrical potential in equation (2) can be expressed using species concentration gradients:

$$\nabla \Psi = -\sum_{i=1}^{N_s} Z_i D_i \nabla c_i / \sum_{i=1}^{N_s} \frac{Z_i^2 F}{RT} D_i c_i. \tag{3}$$

Replacing equation (3) into equation (1) yields the following equation after some algebraic treatments:

$$J_i = -\sum_{k=1}^{N_s} D_{ik} \nabla c_k, \; i = 1, 2, \ldots, N_s, \tag{4}$$

where D_{ik} is the diffusion coefficient of species i in the concentration gradient of species k:

$$D_{ik} = \left(D_i \delta_{ik} - \frac{Z_i Z_k D_i D_k c_i}{\sum_{k=1}^{N_s} Z_k^2 D_k c_k} \right), \tag{5}$$

where δ is the Kronecker symbol. The governing equation for multispecies diffusion can then be derived from equation (4) based on the mass balance for each species in a diffusion domain [e.g., *Lasaga*, 1981; *Miller*, 1967a; *Van Cappellen and Gaillard*, 1996] after including reactions:

$$\frac{\partial c_i}{\partial t} = \nabla \cdot \sum_{k=1}^{N_s} D_{ik} \nabla c_k + r_i, \; i = 1, 2, \ldots, N_s, \tag{6}$$

where r_i is the net production rate of species i from reactions involving species i and t is the time.

[6] The flux equation (equation (4)) and species diffusion model (equation (6)) are derived based on the Nernst-Planck equation (equation (1)). An alternative equation that is based on irreversible thermodynamics [*Cussler*, 1995; *Miller*, 1967a] may also be used to derive diffusion model. The difference between the two approaches will be discussed and evaluated in section 4.3 for uranyl species diffusion under a transient chemical condition. All of the following analysis will be based on equation (6) that is derived from equation (1).

[7] Equation (6) indicates that diffusion of species i depends on the concentration gradients of itself and other species with nonzero charge. The cross-species diffusion coefficient (the second term in equation (5)) results from the fact that positively and negatively charged species have to diffuse coordinately to maintain a net zero electrical current (or charge flux). For a zero-charged species i ($Z_i = 0$), all cross-diffusion coefficients become zero and Eq. 6 becomes a typical Fickian diffusion equation. For a species that is fixed to solid surfaces, such as surface-complexed

species, its self- and cross-diffusion coefficients are all zero and consequently its concentration change can only occur as a result of the reactions.

[8] Equation (6) is formulated for individual species and it requires the rates of all reactions that contribute to species production or consumption (i.e., the r_i term in equation (6)). These reactions include fast reactions that are typically treated as equilibrium reactions and slow ones that are typically represented by kinetic reactions. The rates for fast reactions, such as aqueous- and surface-complexation reactions, are typically not available in literature. It is therefore difficult to directly use Eq. 6 for numerical simulations. To eliminate the requirement of the fast reaction rates in the diffusion equations, chemical species are divided into two sets: components, which are a set of linearly independent species that all other species can be uniquely represented by their linear combination and product species, which are the products of chemical reactions with the components as reactants. The total concentration of chemical component j (T_j) can be described by,

$$T_j = \sum_{i=1}^{N_s} \alpha_{ij} c_i \,, j = 1, 2, \ldots, N_c, \tag{7}$$

where α_{ij} is the stoichiometric coefficient of chemical component j in species i, and N_c is the total number of components. Multiplying α_{ij} to equation (6) and then summing equation (6) for all species yields:

$$\frac{\partial T_j}{\partial t} = \nabla \cdot \sum_{k=1}^{N_s} \left(\sum_{i=1}^{N_s} \alpha_{ij} D_{ik} \right) \nabla c_k + R_j \,, \quad j = 1, 2, \ldots, N_c, \tag{8}$$

where R_j is the net production rate for chemical component j:

$$R_j = \sum_{i=1}^{N_s} \alpha_{ij} r_i, \;\; j = 1, 2, \ldots, N_c. \tag{9}$$

With this treatment, the contributions from equilibrium (fast) reactions to R_j are mutually canceled because equilibrium reactions only rebalance species concentrations, but do not change total component concentrations at any time. Only kinetic reactions have to be considered in R_j in equation (9). Once the total concentrations for all chemical components (T_j, j = 1, 2, … , N_c) were calculated from equation (8), the concentrations for all of the species (free components and product species) can be calculated by linking N_c mass balance equations (equation (7)) with the following mass action equations:

$$\gamma_i c_i = K_i \prod_{j=1}^{N_c} (\gamma_j C_j)^{v_{ij}} \quad i = 1, 2, \ldots, N_s - N_c, \tag{10}$$

where C_j and γ_j are the free species concentration and activity coefficient for chemical component j, K_i and γ_i are the equilibrium constant and activity coefficient for product species i, respectively, and v_{ij} is the stoichiometric coefficient of chemical component j in the equilibrium species reaction for species i. The selection of chemical components from species depends on the need and convenience in numerically solving diffusion problems. N_s-N_c mass action equations (equation (10)) and N_c mass balance equations (equation (7)) were simultaneously solved using the Newton-Raphson method to calculate aqueous and surface complexes speciation in the following analysis.

[9] Equation (8) can be readily solved using an explicit numerical solver to obtain total component concentrations at the next time based on current species concentrations [e.g., *Appelo and Wersin*, 2007]. To use an implicit numerical solver, the right-hand side of equation (8) has to be expressed in terms of total component concentration T_j using equations (7) and (10),

$$\frac{\partial T_j}{\partial t} = \nabla \cdot \left(\sum_{l=1}^{N_c} A_{jl} \nabla T_l \right) + R_j, \tag{11}$$

where A_{jl} is the element in the following matrix:

$$\mathbf{A} = \mathbf{G}\mathbf{B}^{-1}. \tag{12}$$

Matrices **G** and **B** in equation (12) have the following elements:

$$g_{jn} = \sum_{k=1}^{N_s} \sum_{i=1}^{N_s} \alpha_{ij} D_{ik} \frac{\partial c_k}{\partial C_n}, \tag{13}$$

$$b_{nl} = \sum_{k=1}^{N_s} \alpha_{kl} \frac{\partial c_k}{\partial C_n}. \tag{14}$$

The derivative $\partial c_k / \partial C_n$ can be calculated from equation (10). Equation (11) can be solved using an implicit numerical solver. Parameter A_{jl} in equation (11) is generally a nonlinear function of species concentration and its value requires numerical calculations and spatial interpolation at each time step. Updating parameter A_{jl} is the most time-consuming step in solving equation (11). Also, the total concentrations for all components have to be solved simultaneously because they are linked together in equation (11). Nevertheless, the requirement of species self-diffusion coefficients that are often not available for all species in a diffusion system is the main factor preventing use of the fully species- and charge-coupled diffusion model (equation (8) or (11)). Various simplified models are consequently used in the literature to describe species diffusion as listed in Table 1.

[10] The most simplified diffusion model is to assume that all diffusing species have the same diffusion coefficient (D). Under this assumption, the diffusion potential gradient ($\nabla\Psi$) in equations (1) and (3) becomes zero under local charge neutrality condition $\left(\sum_{i=1}^{N_s} Z_i c_i = 0 \right)$, and all of the cross-species diffusion coefficients (the second term in equation (5)) become zero. Consequently, either equation (8) or (11) becomes a Fickian diffusion equation:

$$\frac{\partial T_j}{\partial t} = \nabla \cdot D \nabla \left(\frac{T_j'}{T_j} \right) T_j + R_j \,, \quad j = 1, 2, \ldots, N_c, \tag{15}$$

Table 1. Different Multispecies Diffusion Models

Component-Based Diffusion Equations	Attributes
Model 1 (equation (8)): $\frac{\partial T_j}{\partial t} = \nabla \cdot \sum_{k=1}^{N_s} \left(\sum_{i=1}^{N_s} \alpha_{ij} D_{ik} \right) \nabla c_k + R_j$ or (equations (11)–(14)) $\frac{\partial T_j}{\partial t} = -\nabla \cdot \left(\sum_{l=1}^{M} A_{jl} \nabla T_l \right) + R_j$	Species- and charge-coupled models derived from the Nernst-Planck equation (1). Equation (8) is for explicit numerical solver, and equation (11) with A_{jl} defined by equations (12)–(14) for implicit numerical solver. α_{ik} is the stoichiometric coefficient of component j in species i. D_{ik} (equation (5)) is the cross diffusion coefficient for species i in concentration gradient of species k, and c_k is the concentration of species k. T_j and R_j are the total concentration and reaction rate for component j.
Model 2 (equation (15)): $\frac{\partial T_j}{\partial t} = -\nabla \cdot \left(D \nabla \left[\frac{T_j'}{T_j} \right] T_j \right) + R_j$	Simplified from model 1 by assuming that the self-diffusion coefficients for all dissolved species are the same and constant (D). T_j' is the total dissolved concentration of component j. Other symbols are the same as defined for model 1.
Model 3 (equation (17)): $\frac{\partial T_j}{\partial t} = -\nabla \cdot \left(D_j^c \nabla \left[\frac{T_j'}{T_j} \right] T_j \right) + R_j$	Simplified from model 1 by assuming that self-diffusion coefficients for dissolved species within each chemical component are the same, and each chemical component has its own diffusion coefficient (D_j^c). Other symbols are the same as defined for models 1 and 2.
Model 4 (equation (18)): $\frac{\partial T_j}{\partial t} = \nabla \cdot \left(D_j^c \nabla \left[\frac{T_j'}{T_j} \right] T_j \right) + I_j + R_j$	Alternative model for model 1, but modified from model 3 by adding a secondary migration term I_j (equation (19)) to balance charge in model 3. Other symbols are the same as defined for model 3.
Model 5 (equation (28)) $\frac{\partial T_j}{\partial t} = \nabla \cdot \sum_{k=1}^{N_s} \left(\sum_{i=1}^{N_s} \alpha_{ij} D_{ik} \right) \frac{\nabla a_k}{\gamma_k} + R_j$ or (equations (11), (12), (14), (29)) $\frac{\partial T_j}{\partial t} = -\nabla \cdot \left(\sum_{l=1}^{M} A_{jl} \nabla T_l \right) + R_j$	Alternative species- and charge-coupled models derived from the irreversible thermodynamics in dilute solutions. Equation (28) is for explicit numerical solver, and equation (11) with A_{jl} defined by equations (12), (14), and (29) for implicit numerical solver. a_k is the activity and γ_k is the activity coefficient of species k. Other symbols are the same as defined for model 1.

where T_j' is the total dissolved concentration of component j by assuming zero self-diffusion coefficients for surface-complexed species. The diffusion model with a constant diffusion coefficient (equation (15)) was termed model 2 in the following analysis. Model 2 has been frequently used in diffusion literature including porescale advective diffusion simulations [e.g., *Kang et al.*, 2007; *Li et al.*, 2008; *Tartakovsky et al.*, 2007] and uranyl species diffusion [*Bai et al.*, 2009; *McKinley et al.*, 2006; *Yamaguchi et al.*, 1997]. However, the applicability of the simplified approach has been questioned in literature of rock-water interactions [*Giambalvo et al.*, 2002; *Steefel*, 2007; *Steefel and Maher*, 2009], and has not been evaluated against the fully coupled diffusion model (equation (8) or (11)) in multispecies U(VI) diffusion.

[11] Model 2 can be mathematically viewed as each chemical component has the same diffusion coefficient. The component diffusive flux $D\nabla T_j'$ ($j = 1, \ldots, N_c$) can be calculated by summing diffusive fluxes for individual dissolved species within the component:

$$-D\nabla T_j' = -\sum_{i=1}^{N_{ds}^j} \alpha_{ij} D \nabla c_i, \tag{16}$$

where N_{ds}^j is the number of dissolved species for component j. For a multispecies problem, the total dissolved concentration for component j can be dominated by one or a few species. For example, uranyl speciation consists of many aqueous species (Table 2). However, total dissolved uranyl concentration is often dominated by one or a few species such as uranyl carbonate and/or calcium uranyl carbonate species in groundwater [*Bernhard et al.*, 1996; *Wang et al.*, 2004]. Equation (16) indicates that if the diffusion coefficient D is the same as or close to the self-diffusion coefficients for dominant dissolved species within the component, the component flux calculated using equation (16) can well approximate the flux calculated using the self-diffusion coefficients in model 1. To implement this concept in the diffusion model, we modified equation (15) by assuming that each component has its own diffusion

Table 2. Aqueous and Surface Speciation Reactions Used in Modeling

Reaction	log K (I = 0)	Source[a]
$UO_2^{2+} + H_2O = UO_2\,OH^+ + H^+$	−5.25	1
$UO_2^{2+} + 2H_2O = UO_2\,(OH)_2(aq) + 2H^+$	−12.15	1
$UO_2^{2+} + 3H_2O = UO_2\,(OH)_3^- + 3H^+$	−20.25	1
$UO_2^{2+} + 4H_2O = UO_2\,(OH)_4^{2-} + 4H^+$	−32.40	1
$2UO_2^{2+} + H_2O = (UO_2)_2\,OH^{3+} + H^+$	−2.70	1
$2UO_2^{2+} + 2H_2O = (UO_2)_2\,(OH)_2^{2+} + 2H^+$	−5.62	1
$3UO_2^{2+} + 5H_2O = (UO_2)_3\,(OH)_5^+ + 5H^+$	−15.55	1
$3UO_2^{2+} + 7H_2O = (UO_2)_3\,(OH)_7^- + 7H^+$	−32.20	1
$UO_2^{2+} + CO_3^{2-} = UO_2CO_3(aq)$	9.94	1
$UO_2^{2+} + 2CO_3^{2-} = UO_2(CO_3)_2^{2-}$	16.61	1
$UO_2^{2+} + 3CO_3^{2-} = UO_2(CO_3)_3^{4-}$	21.84	1
$2UO_2^{2+} + CO_3^{2-} + 3H_2O = (UO_2)_2CO_3\,(OH)_3^- + 3H^+$	−0.855	1
$2Ca^{2+} + UO_2^{2+} + 3CO_3^{2-} = Ca_2UO_2(CO_3)_3$	30.70	2
$Ca^{2+} + UO_2^{2+} + 3CO_3^{2-} = CaUO_2(CO_3)_3^{2-}$	27.18	2
$Mg^{2+} + UO_2^{2+} + 3CO_3^{2-} = MgUO_2(CO_3)_3^{2-}$	26.11	2
$CO_3^{2-} + 2H^+ = H_2CO_3(aq)$	16.68	1
$CO_3^{2-} + H^+ = HCO_3^-$	10.33	1
$H_2O = OH^- + H^+$	−14.00	1
$>SOH + UO_2^{2+} + H_2O = >SOUO_2OH + 2H^+$	−5.20	3
$>SOH + UO_2^{2+} + CO_3^{2-} = >SOUO_2HCO_3$	15.68	3

[a]1, *Guillaumont et al.* [2003]; 2, *Dong and Brooks* [2006]; and 3, J. M. Zachara et al. (Rate-limited adsorption/desorption of U(VI) in contaminated, intact subsurface sediment cores from a persistent groundwater plume, submitted to *Geochimica et Cosmochimica Acta*, 2011).

coefficient to account for the difference between different chemical components:

$$\frac{\partial T_j}{\partial t} = \nabla \cdot D_j^c \nabla \left(\frac{T_j'}{T_j} \right) T_j + R_j, \qquad j = 1, 2, \ldots, N_c, \tag{17}$$

where D_j^c is the diffusion coefficient for chemical component j. This model was termed as model 3 in the following analysis.

[12] The component diffusion coefficient may be calculated by averaging self-diffusion coefficients of individual species that contribute to the total component concentration or using the self-diffusion coefficient for the dominant species within the chemical component. The latter approach was used in this study. The approach, however, does not conserve the charge as discussed previously [*Li et al.*, 2006, 2007; *Lichtner and Kang*, 2007]. To compensate for charge imbalance, one can add a secondary migration term (I_j) in equation (17) by comparing equation (17) with the charge-conserved equation (8) to yield:

$$\frac{\partial T_j}{\partial t} = \nabla \cdot D_j^c \nabla \left(\frac{T_j'}{T_j} \right) T_j + I_j + R_j, \qquad j = 1, \ldots, N_c \tag{18}$$

and

$$I_j = \nabla \cdot \sum_{k=1}^{N_s} \left(\sum_{i=1}^{N_s} \alpha_{ij} D_{ik} \right) \nabla c_k - \nabla \cdot D_j^c \nabla \left(\frac{T_j'}{T_j} \right) T_j, \quad j = 1, \ldots, N_c. \tag{19}$$

[13] When D_j^c is properly selected, term I_j is small relative to the first term in the right-hand side of equation (18) as demonstrated in section 4. The secondary migration term (I_j) is induced by the simplification of the multispecies diffusion model (equation (8) or (11)). The diffusion model described by equation (18) was termed as model 4 in this study. Mathematically, it is the same as model 1 (equation (8) or (11)). The difference is in the numerical approaches used in solving the equations. Unlike in the case of equation (8), where an explicit numerical scheme in time is used and in equation (11) case where an implicit scheme is used, here the first term in the right-hand site of equation (18) is solved using the implicit scheme, while term I_j is solved using the explicit scheme in time.

[14] In the following analysis, diffusion model 1 was solved implicitly using equation (11) by sequentially updating parameter A_{jl} at each time step. The results were compared with those from the explicit approach [*Press et al.*, 1992] and identical results were obtained. The implicit approach, however, allowed for using a larger time step [*Press et al.*, 1992]. In addition, the numerical solver was validated against analytical solutions for a system containing two species: 1:1 electrolyte $NaNO_3$ or 1:2 electrolyte $Ca(NO_3)_2$ [*Cussler*, 1995]. Models 2–4 were also solved implicitly. No sequential iterations were required for models 2 and 3 for the cases studied here without kinetic reactions (i.e., $R = 0$ in equations (15) and (17)). For model 4, the secondary migration term (I_j) in equation (18) was calculated iteratively using the last step speciation concentrations. The calculated I_j was then used to solve diffusion equation (18) for total component concentrations, which were used to calculate speciation reactions and I_j again. This process was iterated at each time step until convergence.

[15] Models 1 and 4 (equations (11) and (18)) require self-diffusion coefficients for all species in a diffusion system. The self-diffusion coefficients used in this study (Table 3) were either compiled from the literature [*Lide*, 2003] or calculated from molecular simulations [*Kerisit and Liu*, 2010]. The diffusion coefficient for species $CaUO_2(CO_3)_3^{2-}$, which was a dominant uranyl species under conditions explored in this study, was used as the common diffusion coefficient in model 2. The self-diffusion coefficient for a dominant species within each chemical component was used as the component diffusion coefficient in models 3 and 4. Based on this criterion, the self-diffusion coefficients for species $CaUO_2(CO_3)_3^{2-}$, Ca^{2+}, Mg^{2+}, Na^+, HCO_3^-, HCO_3^-, NO_3^-, and Br^- (Table 3) were used as the component diffusion coefficients for components U(VI), Ca, Mg, Na, CO_2(tot), H, NO_3, and Br, respectively. The self-diffusion coefficient for species HCO_3^- was used for component H because mass balance calculations indicated that proton diffusion was dominated by bicarbonate species. The speciation reactions used in this study were provided in Table 2. The ion activity coefficients required for aqueous and surface speciation reactions (equation (10)) were calculated using the Davies equation.

[16] All diffusion models (equations (8), (11), (14), (17), and (18)) can be directly used for porescale simulations by

Table 3. Self-Diffusion Coefficients and Charge for Multispecies Diffusion Models

Species	D ($cm^2\ s^{-1}$)	Z	Source[a]
H^+	9.31×10^{-5}	1	1
OH^-	5.27×10^{-5}	−1	1
UO_2^{2+}	7.6×10^{-6}	2	2
Na^+	1.33×10^{-5}	1	1
Ca^{2+}	7.9×10^{-6}	2	1
Mg^{2+}	7.1×10^{-6}	2	1
NO_3^-	1.90×10^{-5}	−1	1
Br^-	2.1×10^{-5}	−1	1
HCO_3^-	1.19×10^{-5}	−1	1
CO_3^{2-}	9.23×10^{-6}	−2	1
H_2CO_3(aq)	1.19×10^{-5}	0	1
UO_2CO_3(aq)	6.7×10^{-6}	0	2
$UO_2(CO_3)_3^{2-}$	5.5×10^{-6}	−2	2
$UO_2(CO_3)_3^{4-}$	5.5×10^{-6}	−4	2
UO_2OH^+	7.6×10^{-6}	1	3
$UO_2(OH)_2$(aq)	7.6×10^{-6}	0	3
$UO_2(OH)_3^-$	7.6×10^{-6}	−1	3
$UO_2(OH)_4^{2-}$	7.6×10^{-6}	−2	3
$(UO_2)_2OH^{3+}$	7.6×10^{-6}	3	3
$(UO_2)_2(OH)_2^{2+}$	7.6×10^{-6}	2	3
$(UO_2)_3(OH)_5^+$	7.6×10^{-6}	1	3
$(UO_2)_3(OH)_7^-$	7.6×10^{-6}	−1	3
$CaUO_2(CO_3)_3^{2-}$	5.1×10^{-6}	−2	2
$Ca_2UO_2(CO_3)_3$(aq)	4.6×10^{-6}	0	2
$MgUO_2(CO_3)_3^{2-}$	5.1×10^{-6}	−2	2
$(UO_2)_2CO_3(OH)_3^-$	4.6×10^{-6}	−1	2
>SOH	0.0	0	4
>$SOUO_2OH$	0.0	0	4
>$SOUO_2HCO_3$	0.0	0	4

[a] 1, *Lide* [2003]; 2, *Kerisit and Liu* [2010]; 3, assumed to be the same as for UO_2^{2+}; and 4, assumed to be zero.

explicitly treating solid grain geometry as boundaries. When the models are used to simulate diffusion in porous media (including both pore and solid phases), an apparent tortuosity factor normalized to a characteristic length in the diffusion domain (τ/L^2, where τ is tortuosity, and L is the characteristic length) is typically used to scale self-diffusion coefficients in the aqueous phase to diffusion coefficients in porous media. The apparent tortuosity τ is defined as $\tau = D_p/D_m$, where D_m is the molecular diffusion coefficient and D_p is the diffusion coefficient in porous media. The selection of characteristic length L depends on calculation convenience. Note that in porous media, with low pore connectivity such as in intragranular domains, the apparent tortuosity factor may not be a constant as it may change with diffusion time and distance as a result of effective pore structure changes from grain surfaces toward the interior [*Ewing et al.*, 2010]. The pore connectivity effect was not considered in the following simulations. The characteristic length was taken as the length of a diffusion column when simulating U diffusion in the low permeability materials; and is the particle radius when simulating diffusion-limited U(VI) adsorption and desorption in intragranular regions in the following analysis.

3. Experiments

[17] Stirred flow-cell experiments were performed to evaluate the diffusion-limited U(VI) sorption/desorption process in sediment intragranular domains. Two sediments were collected from the Integrated Field Research Challenge (IFRC) site at the U.S. DOE Hanford's 300 Area, where a field research is ongoing to investigate U(VI) reactive transport. Spectroscopic analysis has revealed that uranium in the sediments existed as adsorbed uranyl carbonate ($>SOUO_2HCO_3$) and hydroxyl ($>SOUOH$) species that are associated with the <2 mm size fraction [*Arai et al.*, 2007; *Liu et al.*, 2008]. These two surface species were used to describe U(VI) surface complexation reactions in this study (Table 2). The surface complexation reactions explicitly account for the effect of H^+ and CO_3^{2-} on U(VI) adsorption. The effect of other chemical components on U(VI) adsorption was considered through aqueous speciation reactions, which influenced uranyl species activity and surface-complexation reactions (Table 2). The intragranular nature of U(VI) residence [*Stubbs et al.*, 2009] and the kinetic behavior of U(VI) release and uptake [*Liu et al.*, 2008, 2009; *Qafoku et al.*, 2005] indicated that intragranular diffusion is a major mechanism controlling U(VI) adsorption and desorption in the Hanford 300 Area sediments. This example provided an excellent scenario to evaluate the multispecies diffusion models as described in section 2.

[18] Experiments were performed using the <2 mm size fraction sieved from two IFRC sediments. Before sieving, the field-textured sediments had been leached with a synthetic groundwater (SGW1, Table 4) in column systems for over 70 pore volumes (PV) to investigate U(VI) desorption. After removal of the residual uranium in the column systems by continuous flushing U-free SGW1, the field-textured sediment was air-dried, collected, and sieved to isolate the <2 mm size fraction for this study. SGW1 with and without a spike of U(VI) (60 ppb) and Br (5 ppm) was used as the injection solution in stirred flow-cell reactors. The chemical composition in the SGW1 mimics that in groundwater at the Hanford 300 Area (Table 4), and was in equilibrium with atmospheric CO_2(g) and calcite. The Br was used as a tracer to evaluate the multispecies diffusion models under a nonreactive condition. Charge coupling was considered in models 1 and 4 to describe the diffusion of negatively charged species Br^-. SGW1 was injected from the bottom of the flow-cell reactor using a HPLC pump at 9.6 mL hr^{-1} with a residence time of 1.3 hr in the reactor. The effluent from the top of the reactor was collected by a fraction collector. A 0.2 μm pore size membrane was fixed on the effluent port to retain the sediment in the reactor. The flow-cell experiments were performed with a solid/water ratio of 260 g L^{-1} continuously mixed by a magnetic stir bar. An intermittent flow and stop-flow (SF) technique with variable SF durations was applied to generate dynamic diffusion gradients for U(VI) adsorption and desorption in the intragranular domains. The Br was measured using a Br electrochemical prober, and U(VI) in the effluents was monitored with a kinetic phosphorescence analyzer with a detection limit of 0.001 μmol L^{-1} (Chemchek Instruments, Richland, WA). Independent experiments were performed and found that important chemical components (Ca, CO_2[tot], and pH) that can affect uranium speciation had negligible changes during the stirred flow-cell experiments.

Table 4. The Composition of Leaching Solutions

	K	Ca	Na	Mg	CO_2(tot)[a]	pH	NO_3
			(mmol)				
SGW1	0.387	0.626	1.39	0.559	1.19	8.12	2.96
SGW2	0.014	0.032	80.7	0	9.78	9.09	69.6

[a]Total dissolved inorganic carbon.

4. Results and Discussion

[19] Two scenarios were considered to evaluate the multispecies diffusion models. The first scenario considered diffusion-limited U(VI) surface-complexation reactions in intragranular regions under steady state solution chemical composition. This diffusion scenario was linked with flow and mixing in the bulk solution to describe the experiment results in the stirred flow-cell system as described in section 3. The second scenario is hypothetical by considering intergranular multispecies U(VI) diffusion in a diffusion column. A similar scenario was experimentally explored previously and the data were reported elsewhere [*Bai et al.*, 2009; *Liu et al.*, 2010]. In this scenario, the sediment was first loaded with U(VI) in equilibrium with the SGW1. The U(VI)-containing sediment was then packed into a diffusion column. To start the diffusion process, the diffusion column was submerged in a U(VI)-free SGW2 with a higher pH and carbonate concentration (Table 4). The SGW2 was allowed to diffuse into the diffusion cell only through one column end. The high pH and carbonate in the SGW2 promoted U(VI) desorption, and subsequently U(VI) diffusion in coupling with major chemicals in the diffusion column. The calculated concentration profiles of U(VI) and major chemicals in the diffusion column were used to evaluate different diffusion models.

4.1. Diffusion-Limited Intragranular U(VI) Surface Complexation

[20] The effluent U(VI) concentrations from the flow-cell reactor showed kinetic behavior of U(VI) sorption and desorption as revealed by their response to the stop-flow events, and their difference from tracer Br curves (Figures 1 and 2). The 16 hr SF event after an injection of 55 mL SGW1, induced the decrease in effluent U(VI) concentration when flow was restarted. This decrease was not observed for tracer Br (Figures 1A and 2A) and reflected the kinetic behavior of grain-scale U(VI) adsorption. The

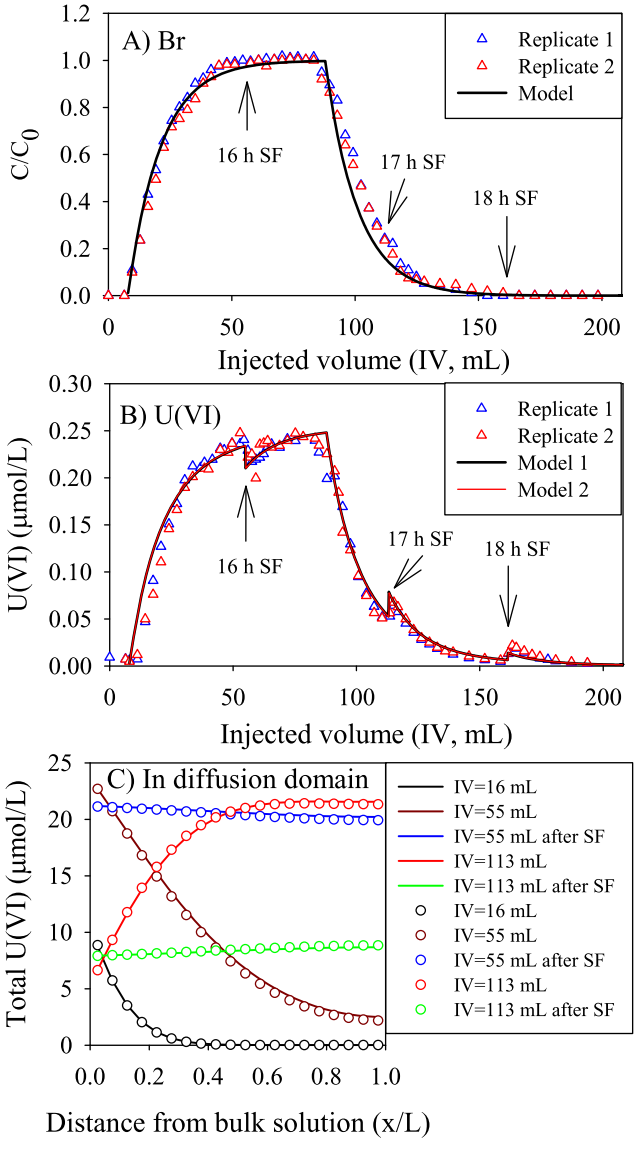

Figure 1. Measured and simulated results from a stirred flow-cell reactor containing sediment 1. (a) effluent Br, (b) effluent U(VI), and (c) total U(VI) in the intragrain domains. In Figures 1a and 1b, the triangles are the experimental results and the lines are the simulated results. In Figure 1c, the lines are the simulated results using model 1 and the circles are the simulated results using model 2. Models 1 and 2 were described in text. SF denotes stop-flow with SF durations inserted.

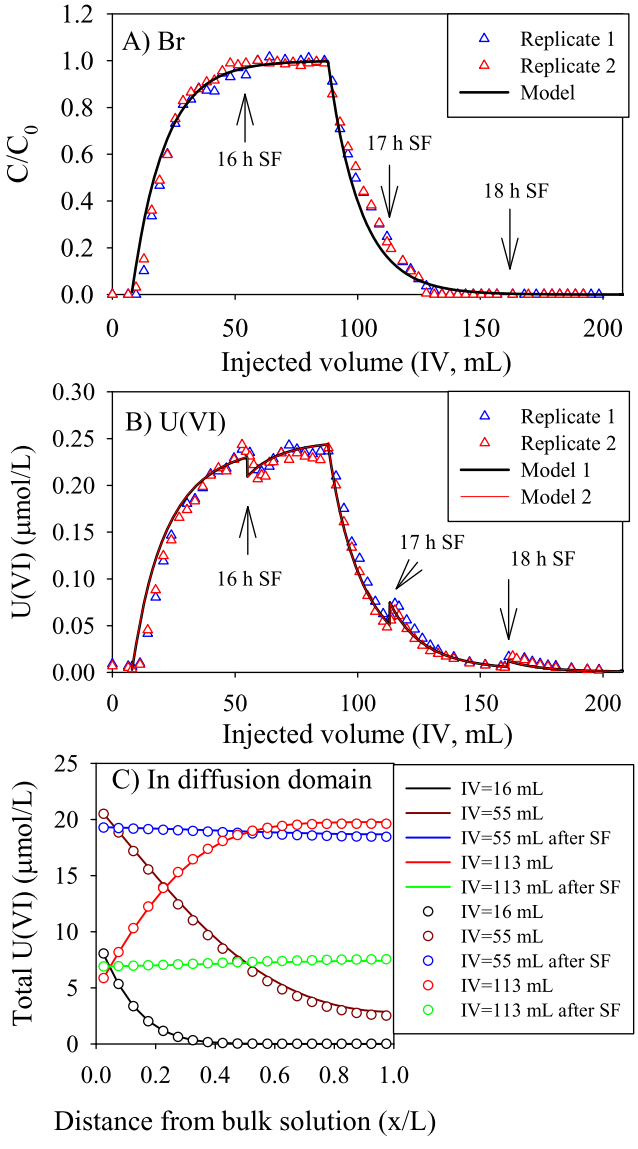

Figure 2. Measured and simulated results from a stirred flow-cell reactor containing sediment 2. (a) effluent Br, (b) effluent U(VI), and (c) total U(VI) in the intragrain domains. In Figures 2a and 2b, the triangles are the experimental results and the lines are the simulated results. In Figure 2c, the lines are the simulated results using model 1 and the circles are the simulated results using model 2. Models 1 and 2 were described in text. SF denotes stop-flow with SF durations inserted.

SF events after 113 and 160 mL SGW1 injection caused a rebounding in effluent U(VI) concentration, which again, was not observed for Br (Figures 1 and 2). These results indicated that the kinetic behavior was only for sorptive U(VI), not for nonreactive tracer Br. As described before, the kinetic behavior of U(VI) adsorption and desorption was attributed to the diffusion-limited surface-complexation reactions within the intragrain regions in the sediment. Br was also expected to have diffused into and out of the intragrain regions during the U(VI) adsorption and desorption phases. However, its effect was not measurable because of the small intragrain pore versus bulk solution volume. The intragranular

pore volume was estimated to be 1.6×10^{-2} cm^3 g^{-1}, which gave a volume ratio of 0.4% intragrain versus bulk solution in the flow-cell reactor calculated using a solid/water ratio of 260 g L^{-1}. The intragranular pore volume was independently estimated based on N_2 sorption measurements and pore volume analysis. The measurable effect of intragranular diffusion on bulk U(VI) concentration was caused by U(VI) surface complexation reactions that significantly increased the intragranular storage capacity as further discussed in the following modeling results.

[21] The effluent data in Figures 1 and 2 were used to evaluate the multispecies diffusion models to describe diffusion-limited U(VI) surface complexation in the intragranular regions. The effluent U(VI) concentration was described using the following equations by linking with the intragranular diffusion models:

$$V_b\left(\frac{dT_j^b}{dt}+V_p\rho_s\frac{d\bar{T}_j}{dt}\right)=F(T_j^{in}-T_j^b),\quad j=1,2,\ldots,N_c, \quad (20)$$

where V_b (cm^3) is the solution volume in the flow-cell reactor, V_p (cm^3 g^{-1}) is the pore volume in solid phase, ρ_s is the solid/water ratio (g cm^{-3}) in the reactor, F is the flow rate (cm^3 min^{-1}), T_j^b and T_j^{in} (mol L^{-1}) are the total concentrations of chemical component j in bulk and influent solutions, respectively, and $\bar{T}_j$ is the average total concentration of chemical component j in the intragranular pore domain, which was calculated by assuming spherical particles:

$$\bar{T}_j=3\int_0^1 T_j r^2 dr, \quad (21)$$

where T_j was calculated from diffusion models as described before.

[22] Model 1 (equation (11)) was first used to link with equations (20) and (21) to describe effluent Br and U(VI) results (Figures 1 and 2). In this model, parameters F/V_b (1.2×10^{-2} min^{-1}) and ρ_s (260 g L^{-1}) were experimentally designed and/or measured, and V_p was determined from the N_2 sorption measurement (1.6×10^{-2} cm^3 g^{-1}) as described before. The total site concentration for U(VI) surface complexation was calculated from a site density of 3.84×10^{-6} mol m^{-2} and a measured intragranular micropore surface area of 1.94 and 1.78 m^2 g^{-1} for sediments 1 (Figures 1) and 2 (Figure 2) cases, respectively. The micropore surface areas were also independently determined from the N_2 sorption data. The only unknown parameter is τ/L^2, which was used to scale aqueous self-diffusion coefficient-to-diffusion coefficient in the solid grain. This parameter was estimated by fitting the effluent U(VI) data in Figures 1 and 2. Nine chemical components: U(VI), Na, Ca, Mg, H, CO_2(tot), NO_3, Br, and >SOH, where >SOH is the surface site symbol, and 29 species were considered in the modeling. These species, their charge, and self-diffusion coefficients are provided in Table 3. As described before, the total concentrations of the chemical components, except U(VI) and Br, were considered as constants in the reactor for this example. All aqueous and surface speciation reactions were assumed to be local equilibrium in the intragranular diffusion domain so that the rate term (R_j) in equation (11) was zero.

[23] Model 1 was able to describe both effluent Br and U(VI) concentrations in both sediments (Figures 1 and 2) with a fitted parameter of $\tau/L^2 = 1$ mm^{-2} or $\tau = 0.25$ assuming $L = 0.5$ mm for averaged particle radius in the sediments. The same fitted τ/L^2 was able to describe the results from both sediments because of their relatively small difference (8%) in surface areas. As expected, the diffusion in the intragranular region had no effect on the calculated effluent Br because of a small intragrain pore volume relative to the bulk solution. For U(VI), surface-complexation reactions (Table 2) significantly increased the intragranular storage capacity. The equilibrium ratio of U(VI) mass in the intragranular regions versus that in the bulk solution in the reactor can be calculated by:

$$\text{ratio}=\frac{\left(C_{UO_2}^{aq}+C_{>SOUO_2OH}+C_{>SOUO_2HCO_3}\right)V_p\rho_s}{C_{UO_2}^{aq}}, \quad (22)$$

where $C_{UO_2}^{aq}$ is the total aqueous U(VI) concentration, $C_{>SOUO_2OH}$ and $C_{>SOUO_2HCO_3}$ are the concentrations for two uranyl surface complexes in the intragrain domain. Within the concentration range for aqueous U(VI) in Figures 1 and 2, the calculated equilibrium ratio is 36% for U(VI). In contrast, the maximum ratio for nonsorbing Br is 0.4%. The high storage capacity for U(VI) in the intragranular regions led to the measurable effect of SF events to U(VI) concentration in the bulk solution.

[24] The SF events had a large effect on intragranular U(VI) concentration distributions in both U(VI) injection and leaching phases (Figures 1C and 2C). The U(VI) concentrations in Figures 1C and 2C are the total concentrations (aqueous and adsorbed species) normalized to aqueous volume in the intragranular domain. The concentration gradient was toward the interior during the U(VI) injection phase (e.g., injection volume [IV] = 16 and 55 mL) and toward the exterior of the diffusion domain during the U(VI) release phase (e.g., IV = 113). The large difference in intragrain diffusion profiles before and after the stop-flow events (after an injection of 55 and 113 mL SGW1) was caused by U(VI) diffusion that significantly decreased its concentration gradient during the SF events. All of these SF durations were less than 1 d, indicating that the intragrain diffusion for U(VI) adsorption and desorption was a relatively fast process. This was in contrast to the previous finding that U(VI) desorption from contaminated sediments at the Hanford 300 Area was a slow process with a half-life of months and years [*Liu et al.*, 2009; *Qafoku et al.*, 2005]. The contrast apparently resulted from the fact that the U(VI) in the contaminated sediments had been in ground for over 40 yr, allowing the contaminant to diffuse into deep diffusion regions. These deep diffusion regions were apparently not accessed by the short-term reactive diffusion as explored here. This contrast also implied that there were two types of pore domains with one domain readily accessible by short-term diffusion and the other domain requiring a long time to access. This dual diffusion domain concept was consistent with a recently developed pore connectivity model in the intragrain regions [*Ewing et al.*, 2010], which revealed two clusters of pores, one near the grain surfaces with faster apparent diffusivity; the other includes those in the interior with relatively slower apparent diffusivity.

[25] Model 2, which used the self-diffusion coefficient of species $CaUO_2(CO_3)_3^{2-}$ for all diffusing species, generated the same effluent U(VI) concentrations (Figures 1B and 2B). The difference in the calculated total U(VI) concentrations in the intragranular regions was also negligible between the two models (Figures 1C and 2C). These results indicated that the fully coupled multispecies diffusion models (equation (11)) can be simplified using equation (15) in a groundwater solution with a steady state major chemical composition. This is because the steady state chemical composition maintained a stable U(VI) aqueous speciation, which was dominated by species $CaUO_2(CO_3)_3^{2-}$ in this case. Consequently, there was a small difference in U(VI) diffusion flux calculated using the two models because the flux contributions from other uranyl species were negligible. Similarly, the other diffusion models (models 3 and 4) can generate the same results as model 1 (data not shown) as long as the diffusion coefficient for species $CaUO_2(CO_3)_3^{2-}$ was used for U(VI) component in these alternative models.

4.2. U(VI) Diffusion Under Transient Chemical Composition

[26] The simplified multispecies diffusion models were further evaluated against model 1 under a transient chemical condition. Figures 3 and 4 showed two snapshots of diffusion profiles of U(VI) and other related species in a diffusion column that was initially in equilibrium with SGW1 containing 0.25 μmol L^{-1} of dissolved U(VI) and corresponding equilibrium-adsorbed U(VI) (2.75 μmol L^{-1}). The porosity in the diffusion column was 0.3 with a bulk solid density of 1.8 g cm^{-3} and U(VI) adsorption site density of 6.5 μmol g^{-1}. The detail experimental setup for the diffusion system was described elsewhere [*Liu et al.*, 2010]. At time zero, one end (x/L = 0) of the diffusion column was in contact with a bulk solution containing U(VI)-free SGW2 (Table 4). The bulk solution volume was assumed to be large enough that its chemical composition was not affected by mass exchange into and out of the diffusion column. The compositional difference between SGW1 and SGW2 created transient diffusion profiles in the diffusion column (Figures 3 and 4), which promoted local U(VI) desorption and diffusion (Figures 3A and 3B). One interesting observation was that the dissolved U(VI) concentration profile had concentration gradients toward both the interior and exterior of the diffusion column at earlier times (e.g., $t = 0.02\ L^2/\tau D_e$, where D_e is the self-diffusion coefficient of species $CaUO_2(CO_3)_3^{2-}$, $L = 10$ cm, and $\tau = 0.2$). This phenomenon was caused by the local U(VI) desorption promoted by the inward diffusion of carbonate and pH, and diffusion-limited removal of dissolved U(VI) from the diffusion column. The dissolved U(VI) concentration gradients not only drove U(VI) diffusion out of the column, but also moved dissolved U(VI) into the interior. A peak in total U(VI) concentration near x/L = 0.4, which was higher than the initial total U(VI) concentration (Figure 3A), reflected this inward diffusion. When local U(VI) desorption was near completion, the two side concentration gradients of dissolved U(VI) disappeared and inward diffusion ceased (e.g., at $t = 0.2\ L^2/\tau D_e$). The macroscopic effect of this inward diffusion is the decrease in the rate of U(VI) release from the diffusion domain to the bulk solution.

[27] Model 2 deviated from model 1 under a transient chemical condition (Figures 3 and 4). The deviation for major chemical components was in proportion to the difference in

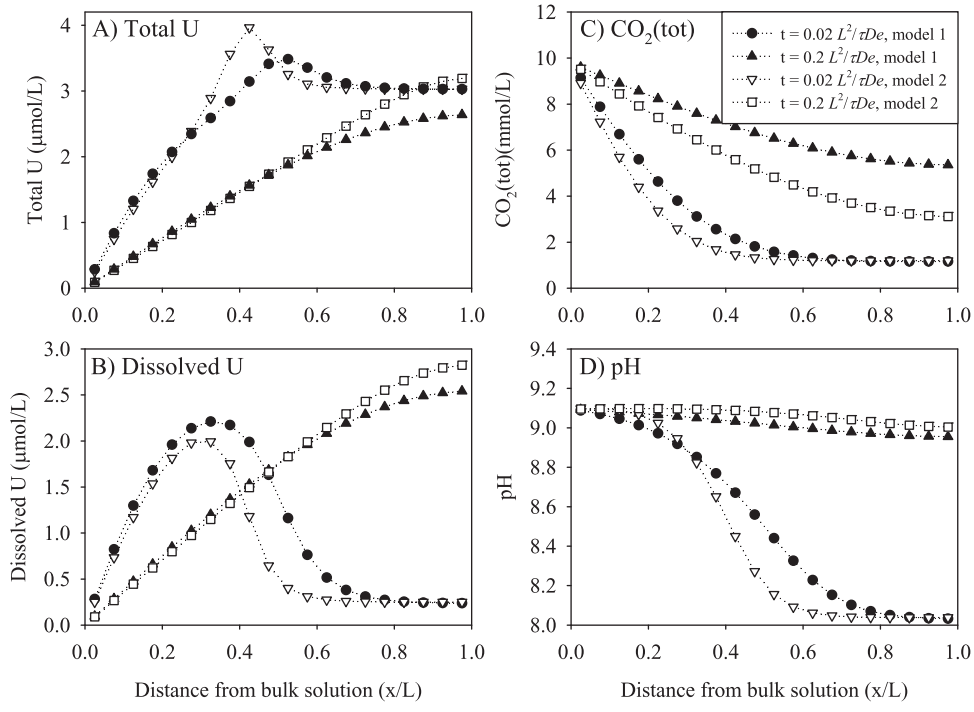

Figure 3. Spatial distribution of calculated concentrations of (a) total U(VI), (b) dissolved U(VI), (c) CO_2(tot), and (d) pH at two times in a diffusion column initially in equilibrium with SGW1 (Table 4) and total 3 μmol L^{-1} U(VI). Bulk solution SGW2 (Table 4) at x/L = 0. Models 1 and 2 were used in the calculations.

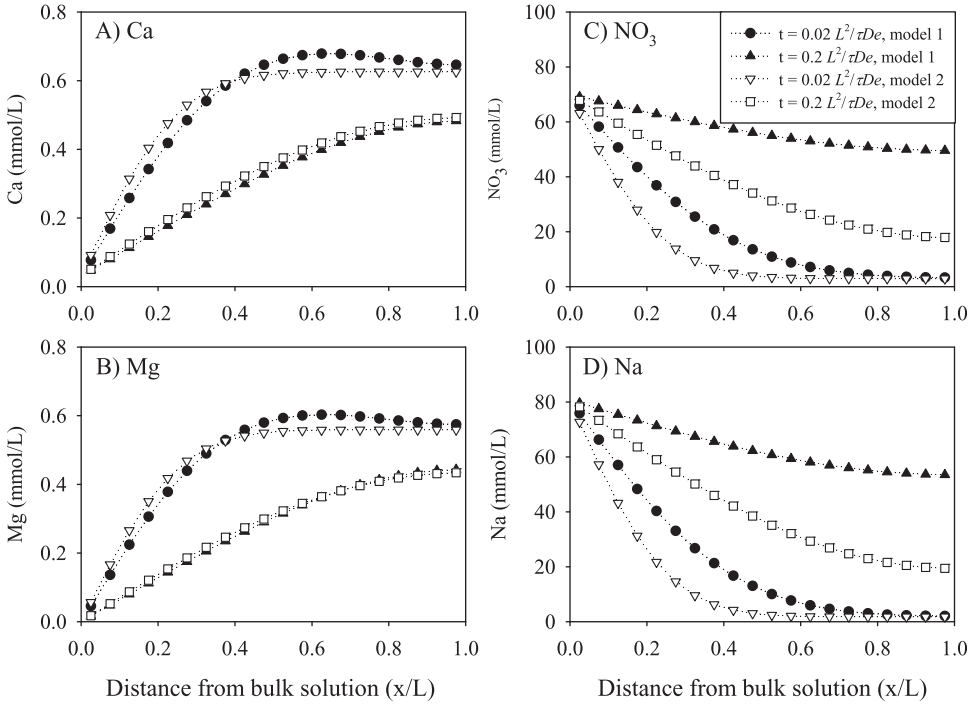

Figure 4. Spatial distribution of calculated concentrations of chemical component Ca (A), Mg (B), NO_3 (C), and Na (D) at two times in a diffusion column initially in equilibrium with SGW1 (Table 4). Bulk solution SGW2 (Table 4) at $x/L = 0$. Models 1 and 2 were used in calculations.

diffusion coefficients used in two models. For example, components Ca and Mg were dominated by free species Ca^{2+} and Mg^{2+}. The self-diffusion coefficients of species Ca^{2+} and Mg^{2+} were close to the diffusion coefficient for species $CaUO_2(CO_3)_3^{2-}$, which was used as the common diffusion coefficient in model 2 (Table 3). Consequently, the difference in Ca and Mg diffusion profiles calculated by the two models was smaller than the components: carbonate, Na, and NO_3 (Figures 3 and 4). This was because the self-diffusion coefficients of carbonate, Na, and NO_3 species were nearly double the common diffusion coefficient used in model 2, and thus the inward migration of these components calculated from model 2 lagged that from model 1. For trace species such as aqueous U(VI) and proton, their diffusion profiles were not only affected by their diffusion coefficients, but more importantly, by speciation reactions. The diffusion front of dissolved U(VI) was significantly affected by U(VI) surface-complexation reactions, which were affected by carbonate and pH diffusion profiles. The slower migration of high bicarbonate and high pH solution toward the interior of the diffusion column as calculated by model 2 delayed U(VI) desorption (Figure 3B), which slowed the overall U(VI) release to the bulk solution (Figure 3A). Behind the U(VI) desorption front, the change in solution chemical composition had a lesser effect on U(VI) aqueous and surface-complexation reactions. Consequently, U(VI) diffusion profiles calculated by two models were almost identical, e.g., from $x/L = 0$ to 0.1 at $t = 0.02\ L^2/\tau D_e$, and from $x/L = 0$ to 0.5 at $t = 0.2\ L^2/\tau D_e$.

[28] The pH diffusion profile was mainly affected by local speciation, which was controlled by the diffusion of major species, in this case, carbonate species. Equation (7) for total proton concentration was dominated by carbonate species and thus the total proton concentration profile (data not shown) was nearly identical to that of CO_2(tot) (Figure 3). The carbonate species rebalanced their speciation by consuming protons as they migrated from the bulk solution with a higher ratio of CO_3^{2-}/HCO_3^- into the diffusion column initially with a relatively lower ratio of CO_3^{2-}/HCO_3^-. A slight change in the carbonate species ratio had a major effect on pH because of the high concentration ratio of carbonate versus free proton, so that pH diffusion front (Figure 3D) advanced more quickly than CO_2(tot) (Figure 3C). The slower migration of CO_2(tot), calculated by model 2, caused a slower migration of the pH diffusion front as compared to the model 1 case at an earlier time (e.g., $t = 0.02\ L^2/\tau D_e$) (Figure 3D). The faster self-diffusion coefficients of H^+ and OH^- (Table 3) may also have affected the faster migration of pH in the model 1 case. However, such effect was minor as shown later in the discussion for model 3 results. When pH in the diffusion domain was close to equilibrium (i.e., equal to that in bulk solution), for example, at locations near the bulk solution at early time ($t = 0.02\ L^2/\tau De$) and entire diffusion domain at later time ($t = 0.2\ L^2/\tau De$), model 2 produced a slightly higher pH than that from model 1. This phenomenon was attributed to the charge-coupling effect. In the case for model 1, positively charged H^+ was carried and negatively charged OH^- was repulsed by the inward diffusion of negatively charged major species, NO_3^-, CO_3^{2-}, and HCO_3^-. The net result of this charge coupling was to slow pH migration into the diffusion domain. This charge coupling effect was, however, secondary compared with speciation reactions that consumed or released H^+. Its effect became observable only when the system was close

to equilibrium when speciation reaction effects diminished. The charge-coupling effect cannot be simulated by model 2, where only speciation reactions were considered. The charge-coupling effect will be further discussed in Ca and Mg diffusion.

[29] Both Ca and Mg diffusion profiles showed a peak concentration near $x/L = 0.6$ (Figures 4A and 4B). The peak concentration was higher than the initial Ca or Mg concentration in the diffusion column and that in the bulk solution, showing their accumulation against the concentration gradient. This accumulation demonstrated that the charge-coupling effect was caused by the faster diffusion of negatively charged NO_3 and carbonate species toward the interior of the diffusion column. Although Na diffusion partially compensated for the charge deficiency, it was not enough to balance the local charge because of its smaller self-diffusion coefficient than those of the negatively charged species (Table 3). This charge imbalance pushed inward the diffusion of Ca^{2+} and Mg^{2+} by overcoming their concentration gradients. The charge-carrying diffusion was, however, secondary because the accumulation process increased concentration gradients that enhanced subsequent mass dissipation. The charge coupling effect diminished when the negative charge flux toward the interior decreased at later times as concentration gradients became less steep. The charge-coupling effect was again, not observed when model 2 was used.

[30] A comparison of diffusion profiles calculated by models 1 and 2 indicated that the two models generated similar results when the common diffusion coefficient used in model 2 was close to the self-diffusion coefficients used in model 1 such as in Ca and Mg cases.The two models deviated significantly when two models used different diffusion coefficients for dominant species such as for Na, NO_3, and carbonate cases. This observation suggested that simulation results would improve significantly if a component-specific diffusion coefficient was used to replace the common diffusion coefficient for all of the components in model 2. This treatment converts model 2 to model 3 (equation (17)) with the component-specific diffusion coefficients described before. As expected, model 3 significantly improved the simulations for NO_3, CO_2(tot), and Na (Figures 5 and 6) as compared to model 2. The improvement for the major components also improved simulations for trace components [U(VI) and pH] for reasons discussed before. Model 3, however, was not able to simulate the charge coupling effect as shown for Ca and Mg (Figures 6A and 6B).

[31] Minor difference between models 1 and 3 existed because charge conservation was not enforced in model 3. If a more accurate simulation is required and if self-diffusion coefficients are available for all species, diffusion model 4 can be used to correct the charge imbalance in model 3 by adding a secondary migration term (equation (19)). The results generated from model 4 were identical to those from model 1 (data not shown). As a trade-off, the calculation of this secondary migration term would add additional computational effort. However, compared with the model 1 case, model 4 used ~50% less computational time because it avoids the time-consuming matrix inversion and matrix operation procedures that were required for the model 1 approach. For cases when self-diffusion coefficients

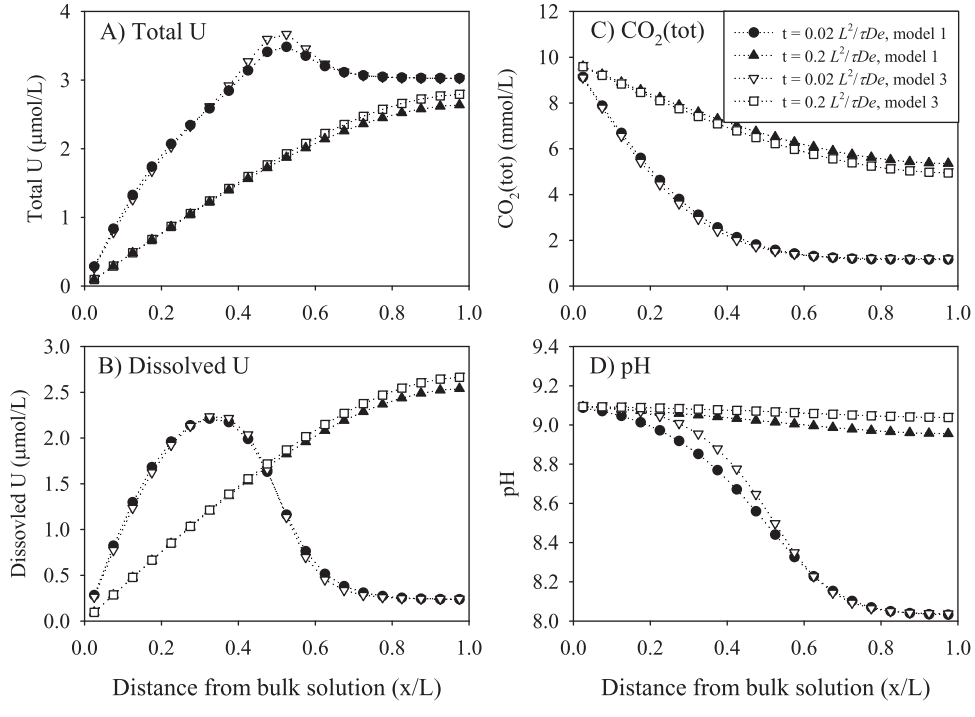

Figure 5. Spatial distribution of calculated concentrations of total U(VI) (A), dissolved U(VI) (B), CO_2(tot) (C), and pH (D) at two times in a diffusion column initially in equilibrium with SGW1 (Table 4) and total 3 μmol L^{-1} U(VI). Bulk solution SGW2 (Table 4) at $x/L = 0$. Models 1 and 3 were used in calculations.

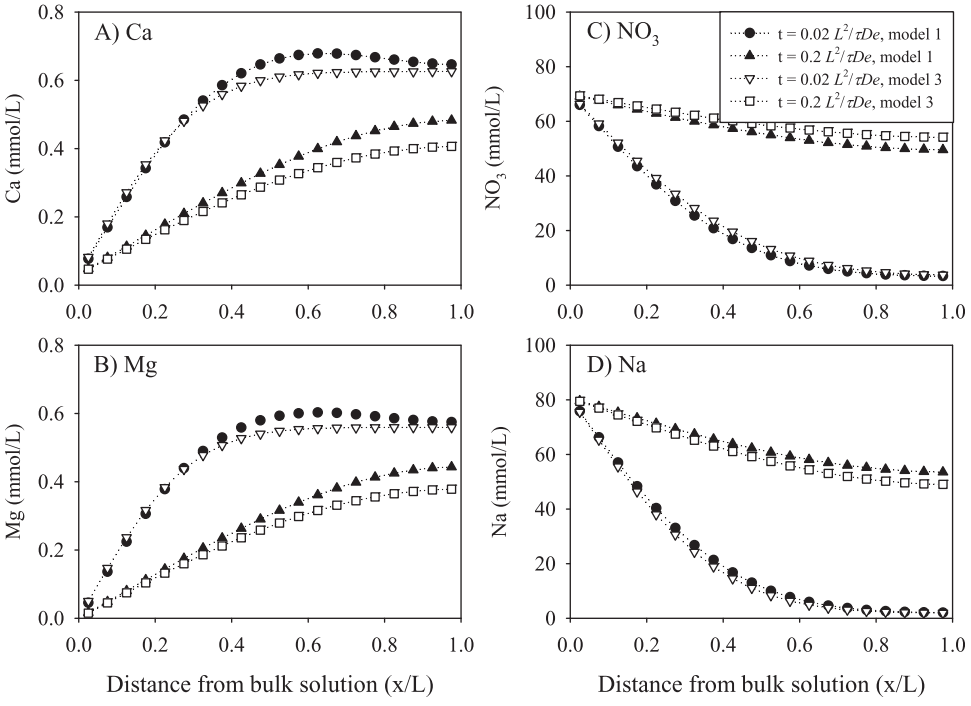

Figure 6. Spatial distribution of calculated concentrations of chemical component Ca (A), Mg (B), NO_3 (C), and Na (D) at two times in a diffusion column initially in equilibrium with SGW1 (Table 4). Bulk solution SGW2 (Table 4) at $x/L = 0$. Models 1 and 3 were used in calculations.

are not available for all species, model 3 would be a better approximation to the fully species- and charge-coupled diffusion model as compared to model 2.

4.3. Effect of Ion Activity Coefficient Gradients

[32] Diffusion models 1–4 in Table 1 are formulated starting from the Nernst-Planck ionic flux equation (1). While equation (1) is the most used in investigating ion diffusion and mass transfer in electrolytes [*Bard and Faulkner*, 2001; *Cussler*, 1995; *Zheng and Wei*, 2011], an alternative equation based on irreversible thermodynamics may also be used to describe ionic flux [*Cussler*, 1995; *Miller*, 1967a]:

$$J_i = \sum_{j=1}^{N_s} l_{ij} X_j, \tag{23}$$

where l_{ij} is the Onsager phenomenological coefficient, and X_j is the thermodynamic force on species i:

$$X_j = -RT\nabla \ln a_j - Z_i F \nabla \Psi, \tag{24}$$

where a_j is the activity of species j. In dilute solutions, the off-diagonal phenomenological coefficients can be neglected (i.e., $l_{ij} = 0$, $i \neq j$), and the diagonal phenomenological coefficient is proportional to concentration (c_i) and mobility (u_i) of species i [*Felmy and Weare*, 1991; *Miller*, 1967b]. Equation (23) then becomes:

$$J_i = -c_i u_i (RT\nabla \ln a_i + Z_i F \nabla \Psi). \tag{25}$$

The aqueous species mobility is related to its self-diffusion coefficient through an Einstein relationship $D_i = RTu_i$, which leads to:

$$J_i = -c_i D_i \nabla \ln a_i - \frac{Z_i F}{RT} D_i c_i \nabla \Psi. \tag{26}$$

Using the relationship of $a_i = \gamma_i c_i$, equation (26) becomes:

$$J_i = -D_i \nabla c_i - \frac{Z_i F}{RT} D_i c_i \nabla \Psi - D_i c_i \frac{\nabla \gamma_i}{\gamma_i}. \tag{27}$$

The difference of equation (27) from equation (1) is the activity coefficient gradient term (third term in the right-hand side of equation (27)). Starting with equation (26), and using the same approach as the derivation for equation (8), the reactive diffusion equation for total chemical component j has the following form:

$$\frac{\partial T_j}{\partial t} = \nabla \cdot \sum_{k=1}^{N_s} \left(\sum_{i=1}^{N_s} \alpha_{ij} D_{ik} \right) \frac{\nabla a_k}{\gamma_k} + R_j. \tag{28}$$

The parameters α_{ij} and D_{ik} are the same as described before. Equation (28) can be directly used for an explicit numerical solver. For an implicit scheme, equation (11) can still be used after modifying its coefficients described by equation (13):

$$g_{jn} = \sum_{k=1}^{N_s} \sum_{i=1}^{N_s} \alpha_{ij} D_{ik} \frac{\partial a_k}{\gamma_k \partial C_n}, \tag{29}$$

where derivative $\frac{\partial a_k}{\partial C_n}$ can be calculated from equation (10). Either equation (28) or equation (11) with their parameters described by equations (12), (14), and (29) was termed model 5 (Table 1) in the following description.

[33] The diffusion term in the right-hand side of equation (28) can be separated into two terms:

$$\nabla \cdot \sum_{k=1}^{N_s} \left(\sum_{i=1}^{N_s} \alpha_{ij} D_{ik} \right) \frac{\nabla a_k}{\gamma_k} = \nabla \cdot \sum_{k=1}^{N_s} \left(\sum_{i=1}^{N_s} \alpha_{ij} D_{ik} \right) \nabla c_k + \nabla \cdot \sum_{k=1}^{N_s} \left(\sum_{i=1}^{N_s} \alpha_{ij} D_{ik} \right) \frac{c_k \nabla \gamma_k}{\gamma_k}. \quad (30)$$

The first right-hand side term in equation (30) is the same as the diffusion term in equation (8), and the second term is the diffusion driven by the activity coefficient gradients. To evaluate the effect of the activity coefficient gradients on multispecies diffusion, model 5 was compared with model 1 for the case of uranyl species diffusion under the transient chemical condition (Figures 7 and 8). In this case, the ionic strength difference between the bulk solution (80 mM) and the initial solution in the porous media (5 mM) generated an activity coefficient gradient in the diffusion column. Both explicit and implicit numerical schemes were tried, and they showed no difference. For this specific example, the implicit scheme showed no advantage because a large diffusion domain (0.1 m) was involved, which allowed the use of a large time step in the explicit numerical scheme.

[34] Figures 7 and 8 demonstrated that the activity coefficient gradients had only a minor effect on the diffusion of all of the calculated solutes. The difference for ions with a larger concentration (CO_2[tot], NO_3, and Na) was especially smaller. As described before, a slight difference in the major chemical concentrations, such as carbonate, could lead to a relatively larger difference in trace species. This effect was manifested again for pH and dissolved U concentration. The relatively larger pH difference was caused by the smaller difference in carbonate concentration, and the pH difference in turn affected the calculated dissolved U concentrations. The total U concentration profiles, however, showed less effect from the activity coefficient gradient. The charge-coupling effect as demonstrated for Ca and Mg in model 1 was diminished by incorporating the activity coefficient gradient. This was demonstrated by the smaller concentration peaks calculated by model 5 for Ca and Mg at $t = 0.02\ L^2/\tau D_e$ than those calculated by model 1 (Figures 8A and 8B). The diminished effect of the charge coupling was caused by the direction of the activity coefficient gradients, which was opposite to the direction of the concentration gradients of the charge-carrying, negatively charged species (NO_3 and carbonate). The opposite gradient directions for activity coefficient and species concentrations also explained the slightly slower diffusion of CO_2(tot), NO_3, and Na when the activity coefficient gradients were included in the modeling (Figures 7C, 8C, and 8D). Overall, the results in Figures 7 and 8 indicate that the alternative diffusion models with or without considering the effect of the activity coefficient gradient had only a minor difference in calculating the species diffusion

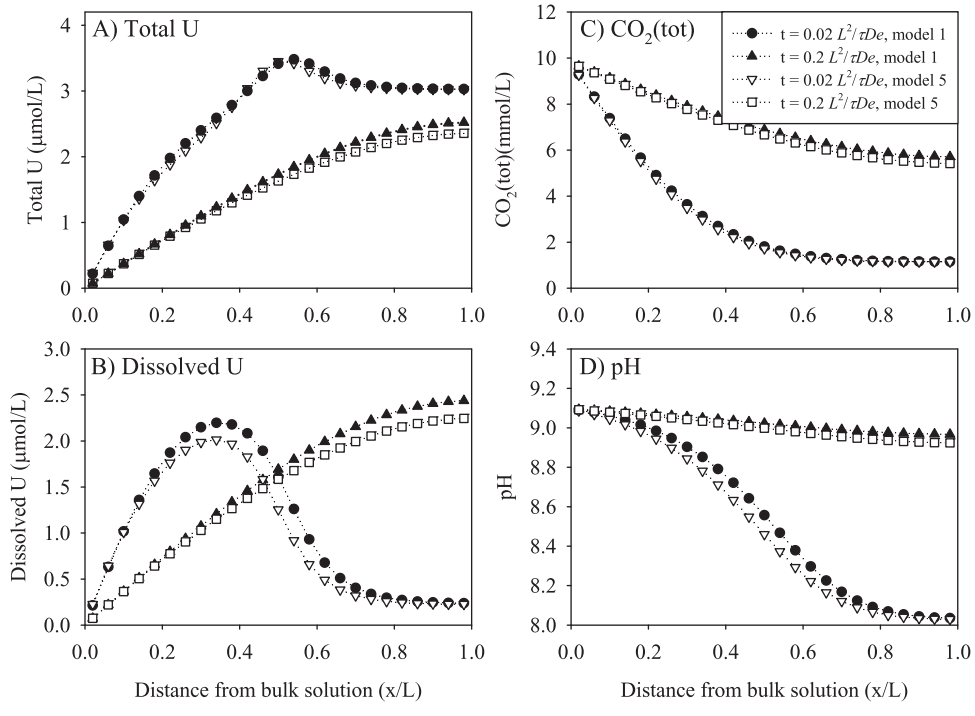

Figure 7. Spatial distribution of calculated concentrations of total U(VI) (A), dissolved U(VI) (B), CO_2(tot) (C), and pH (D) at two times in a diffusion column initially in equilibrium with SGW1 (Table 4) and total 3 μmol L^{-1} U(VI). Bulk solution SGW2 (Table 4) at $x/L = 0$. Models 1 and 5 were used in calculations.

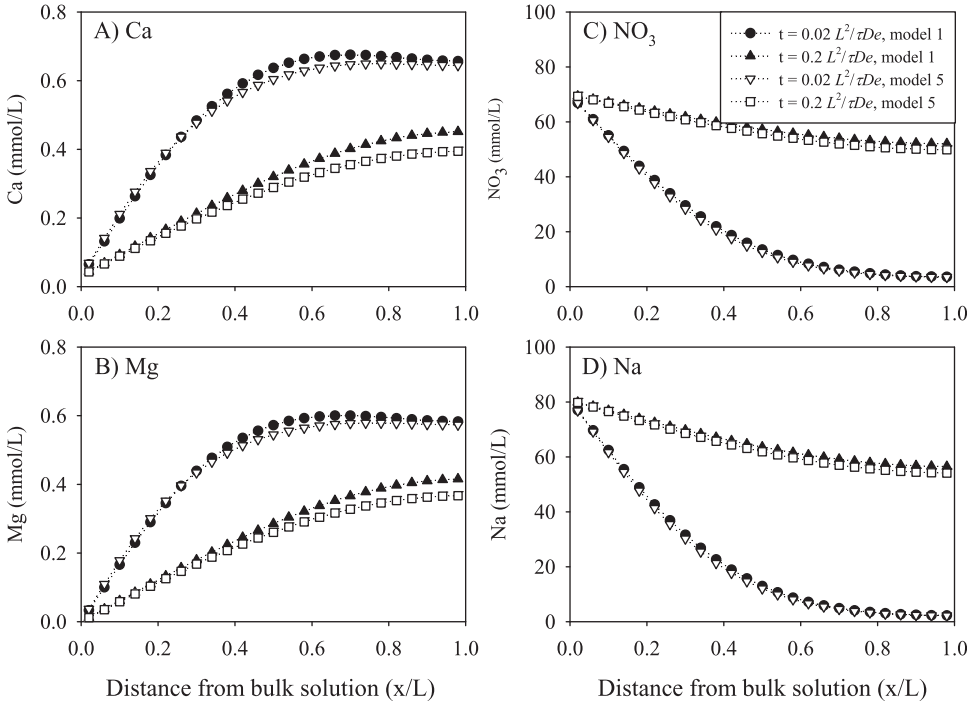

Figure 8. Spatial distribution of calculated concentrations of chemical component Ca (A), Mg (B), NO_3 (C), and Na (D) at two times in a diffusion column initially in equilibrium with SGW1 (Table 4). Bulk solution SGW2 (Table 4) at $x/L = 0$. Models 1 and 5 were used in calculations.

for the explored case. This difference is negligible in comparison with potential errors caused by model 2, where all species diffusion coefficients are treated as a constant (Figures 3 and 4). The effect of the ionic activity coefficient gradient is, however, expected to increase with increasing difference in the ionic strength between the initial and influent solutions.

5. Conclusions and Implication

[35] Diffusion-limited processes are common in those natural environments where groundwater flow is slow or negligible, where chemical reactions are rate-limited by reactant supply and/or reaction product removal, and where mass exchange is controlled by diffusive mixing. Five types of diffusion models were formulated, compared, and discussed in this study to describe multispecies diffusion in porous media. Using uranyl diffusion as examples, this study demonstrated that multispecies diffusion was affected by various factors including self-diffusion coefficients, concentration gradients, charge fluxes, and species and charge coupling through mass actions and charge neutrality condition, as well as the activity coefficient gradients. Proper selection of self-diffusion coefficients was the most important factor for simulating major chemical diffusion, while species reactions and self-diffusion coefficients were the important factors in modeling the diffusion of trace chemicals such as proton and uranyl. The charge coupling to maintain local charge neutrality and the effect of activity coefficient gradients were secondary for the cases studied here. A diffusion model, with a properly selected common diffusion coefficient for all species (i.e., model 2), well approximated a fully coupled multispecies diffusion model when all speciation reactions were incorporated and when major chemical composition was not a spatial function. Under a transient chemical condition, a diffusion model with a constant diffusion coefficient for each component (i.e., model 3) provided a good description of multispecies diffusion at the expense of charge balance that only slightly affected the concentration profiles. Model 3 is consequently recommended as an effective diffusion model when diffusion coefficients for all species are not available and/or when charge conservation is not an important consideration. Another advantage with model 3 is that it can be readily implemented in porescale simulations using numerical schemes such as the lattice Boltzmann model (LBM), where the diffusion coefficient for each component has to be treated as a constant to derive a relaxation time that is required to implement LBM in multispecies reactive transport [*Kang et al.*, 2007]. The fully coupled model is not treatable for LBM and is difficult to numerically implement in other porescale modeling approaches [*Li et al.*, 2006; *Tartakovsky et al.*, 2007]. An additional advantage of using model 3 is that it can be readily improved by adding a secondary migration term (equation (19)) when all species self-diffusion coefficients become available.

[36] The diffusion-limited U(VI) surface complexation has previously been attributed to the time-dependent U(VI) desorption process in sediments containing intragrain U(VI) [*Liu et al.*, 2008, 2009]. This time-dependent process was previously described using a multirate model to approximate the diffusion-limited processes [*Liu et al.*, 2009; *Qafoku et al.*, 2005]. The multirate model assumed that the intragrain regions consist of discrete domains or sites that were in mass exchange with bulk solution. The rate of the mass exchange was described using a first-order kinetics that was driven by the chemical disequilibrium between

intragrain and bulk solutions. The results in Figures 1 and 2 demonstrate that U(VI) adsorption was also a kinetic process that was explicitly described using a diffusion-based model. While a multirate model can also describe the results in Figures 1 and 2 by fitting the multirate parameters (data not shown), the diffusion models provide additional insights into the U(VI) and other chemical concentration evolution in the diffusion domains under transient chemical conditions (e.g., Figures 3 and 4). Such local concentration changes cannot be modeled using the multirate model. Another shortcoming for the multirate model is that it cannot simulate the local inward diffusion of dissolved U(VI) when the overall thermodynamic driving force is for U(VI) desorption. This inward diffusion may become an important factor for porous media containing a large-scale diffusion zone where the inward diffusion can significantly increase the residence time of solutes and contaminants in these zones and consequently slow the overall rate of their release to nearby advective domains.

[37] **Acknowledgments.** This research was supported by the U.S. Department of Energy (DOE) Biological and Environmental Research (BER) Division through the Subsurface Biogeochemical Research Program (SBR) Science Focus Area (SFA) program at Pacific Northwest National Laboratory (PNNL). A portion of the research was performed using the Environmental Molecular Science Laboratory (EMSL), a national scientific user facility sponsored by the DOE-BER and located at PNNL. PNNL is operated for the DOE by the Battelle Memorial Institute under contract DE-AC06-76RLO 1830. We thank reviewers and an associate editor for valuable comments and suggestions.

References

Appelo, C. A. J., and P. Wersin (2007), Multicomponent diffusion modeling in clay systems with application to the diffusion of tritium, iodide, and sodium in Opalinus Clay, *Environ. Sci. Technol.*, *41*, 5002–5007.

Arai, Y., M. A. Marcus, N. Tamura, J. A. Davis, and J. M. Zachara (2007), Spectroscopic evidence for uranium bearing precipitates in vadose zone sediments at the Hanford 300-area site, *Environ. Sci. Technol.*, *41*, 4633–4639.

Bai, J., C. Liu, and W. P. Ball (2009), Study of sorption-retarded U(VI) diffusion in Hanford silt/clay material, *Environ. Sci. Technol.*, *43*, 7706–7711.

Ball, W. P., and P. V. Roberts (1991), Long-term sorption of halogenated organic chemicals, Part 2. Intraparticle diffusion, *Environ. Sci. Technol.*, *25*(7), 1237–1249.

Ball, W. P., C. Liu, G. Xia, and D. F. Young (1997), A diffusion based interpretation of tetrachloroethene and trichloroethene concentration profiles in a groundwater aquitard, *Water Resour. Res.*, *33*(12), 2741–2758.

Bard, A. J., and L. R. Faulkner (2001), *Electrochemical Methods: Fundamental and Applications*, 718 pp., John Wiley, N. Y.

Bernhard, G., G. Geipel, V. Brendler, and H. Nitsche (1996), Speciation of uranium in seepage waters of a mine tailing pile studied by time-resolved laser-induced fluorescence spectroscopy (TRLFS), *Radiochim. Acta*, *74*, 87–91.

Brusseau, M. L. (1991), Application of a multiprocess nonequilibrium sorption model to solute transport in a stratified porous medium, *Water Resour. Res.*, *27*, 589–595.

Cunningham, J. A., C. J. Werth, M. Reinhard, and P. V. Roberts (1997), Effects of grain-scale mass transfer on the transport of volatile organics through sediments 1. Model development, *Water Resour. Res.*, *33*, 2713–2726.

Cussler, E. L. (1995), *Diffusion: Mass Transfer in Fluid Systems*, 525 pp., Cambridge Univ. Press, Cambridge, U. K.

Dong, W., and S. C. Brooks (2006), Determination of the formation constants for ternary complexes of uranyl and carbonate with alkaline earth metal (Mg^{2+}, Ca^{2+}, Sr^{2+}, and Ba^{2+}) using anion exchange method, *Environ. Sci. Technol.*, *40*, 4689–4695.

Ewing, R. P., Q. Hu, and C. Liu (2010), Scale dependence of intragranular porosity, tortuosity, and diffusivity, *Water Resour. Res.*, *46*, W06513, doi:10.1029/2009WR008183.

Felmy, A. R., and J. H. Weare (1991), Calculation of multicomponent ionic diffusion from zero to high concentration: I. The system Na-K-Ca-Mg-SO_4-H_2O at 25°C, *Geochim. Cosmochim. Acta*, *55*, 113–131.

Giambalvo, E. R., C. I. Steefel, A. T. Fisher, N. D. Rosenberg, and C. G. Wheat (2002), Effect of fluid-sediment reaction on hydrothermal fluxes of major elements, eastern flank of the Juan de Fuca Ridge, *Geochim. Cosmochim. Acta*, *66*, 1739–1757.

Grathwohl, P. (1998), *Diffusion in Natural Porous Media: Contaminant Transport, Sorption/Desorption and Dissolution Kinetics*, 224 pp., Kluwer, Boston, Mass.

Guillaumont, R., T. Fanghänel, V. Neck, J. Fuger, D. A. Palmer, I. Grenthe, and M. H. Rand (2003), *Update on the Chemical Thermodynamics of Uranium, Neptunium, Plutonium, Americium and Technetium*, 970 pp., Elsevier, Amsterdam, Netherlands.

Hart, T. D., R. J. Hill, P. M. Glover, J. M. Lynch, and A. H. L. Chamberlain (2001), Effect of a range of microbial polysaccharides on the diffusion of manganese ions using spatially resolved NMR relaxometry, *Enzyme Microb. Tech.*, *28*, 370–375.

Kang, Q., P. C. Lichtner, and D. Zhang (2007), An improved lattice Boltzmann model for multicomponent reactive transport in porous media at the pore scale, *Water Resour. Res.*, *43*, W12S14, doi:10.1029/2006WR005551.

Kerisit, S., and C. Liu (2010), Molecular dynamics calculations of aqueous uranyl carbonate species diffusion, *Geochim. Cosmochim. Acta*, *74*, 4937–4952.

Lasaga, A. C. (1981), Influence of diffusion coupling on diageneric concentration profiles, *Am. J. Sci.*, *281*, 553–575.

Li, L., C. A. Peters, and M. A. Celia (2006), Upscaling geochemical reaction rates using pore-scale network modeling, *Adv. Water Res.*, *29*, 1351–1370.

Li, L., C. A. Peters, and M. A. Celia (2007), Reply to "Comment on upscaling geochemical reaction rates using pore-scale network modeling" by P. C. Lichtner and Q. Kang, *Adv. Water Res.*, *30*, 691–695.

Li, L., C. I. Steefel, and L. Yang (2008), Scale dependence of mineral dissolution rates within single pores and fractures, *Geochim. Cosmochim. Acta*, *72*, 360–377.

Lichtner, P. C. (1996), Continuum formulation of multicomponent-multiphase reactive transport, in *Reactive Transport in Porous Media; Reviews in Mineralogy*, edited by, P. C. Lichtner and C. I. Steefel, pp. 1–81, Mineralogic Soc. of America, Chantilly, VA.

Lichtner, P. C., and Q. Kang (2007), Comment on "Upscaling geochemical reaction rates using pore-scale network modeling" by Li, Peters, and Celia, *Adv. Water Res.*, *30*, 686–690.

Lide, D. R. (2003), *Handbook of Chemistry and Physics*, 2664 pp., CRC Press, Boca Raton, Fla.

Liu, C. X. (2007), An ion diffusion model in semi-permeable clay materials, *Environ. Sci. Technol.*, *41*, 5403–5409.

Liu, C. X., and W. P. Ball (2002), Back diffusion of chlorinated solvent contaminants from a natural aquitard to a remediated aquifer under well-controlled field conditions: Predictions and measurements, *Ground Water*, *40*(2), 175–184.

Liu, C. X., J. M. Zachara, A. R. Felmy, and Y. A. Gorby (2004), An electrodynamics-based model for ion diffusion in microbial polysaccharides, *Colloids Surf. A and B*, *38*, 55–65.

Liu, C. X., J. M. Zachara, W. Yantansee, P. D. Majors, and J. P. McKinley (2006), Microscopic reactive diffusion of uranium in the contaminated sediments at Hanford, USA, *Water Resour. Res.*, *42*, W12420, doi:10.1029/2006WR005031.

Liu, C. X., J. M. Zachara, N. P. Qafoku, and Z. Wang (2008), Scale-dependent desorption of uranium from contaminated subsurface sediments, *Water Resour. Res.*, *44*, W08413, doi:10.1029/2007WR006478.

Liu, C. X., Z. Shi, and J. M. Zachara (2009), Kinetics of uranium(VI) desorption from contaminated sediments: Effect of geochemical conditions and model evaluation, *Environ. Sci. Technol.*, *43*, 6560–6566.

Liu, C. X., L. Zhong, and J. M. Zachara (2010), Uranium(VI) diffusion in low-permeability subsurface materials, *Radiochimica Acta*, *98*, 719–726.

Mafe, S., J. Pellicer, and V. M. Aguilella (1986), Ionic transport and space charge density in electrolyte solutions as described by Nernst-Planck and Poisson equations, *J. Phys. Chem.*, *90*, 6045–6050.

Malusis, M. A., and C. D. Shackelford (2002), Coupling effects of during steady-state solute diffusion through a semipermeable clay membrane, *Environ. Sci. Technol.*, *36*, 1312–1319.

McKinley, J. P., J. M. Zachara, C. Liu, and S. M. Heald (2006), Microscale controls on the fate of contaminant uranium in the vadose zone, Hanford site, Washington, *Geochim. Cosmochim. Acta*, *70*, 1873–1887.

Miller, C. T., and J. A. Pedit (1992), Use of a reactive surface-diffusion model to describe apparent sorption-desorption hysteresis and abiotic degradation of Lindane in a subsurface material, *Environ. Sci. Technol.*, *26*, 1417–1427.

Miller, D. G. (1967a), Application of irreversible thermodynamics to electrolyte solutions. III. Equations for isothermal vector transport processes in n-component systems, *J. Phys. Chem.*, *71*, 3588–3592.

Miller, D. G. (1967b), Application of irreversible thermodynamics to electrolyte solutions. II. Ionic coefficients l_{ij} for isothermal vector transport processes in ternary systems, *J. Phys. Chem.*, *71*, 616–632.

Nomura, K., and T. Sakata (2001), Diffusion potential is induced by coupled transport of ions through liquid membrane: Nonlinear response to pH changes in a reverse permeation system, *J. Membr. Sci.*, *194*, 177–184.

Parker, B. L., J. A. Cherry, and S. W. Chapman (2004), Field study of TCE diffusion profiles below DNAPL to assess aquitard integrity, *J. Contam. Hydrol.*, *74*, 197–230.

Press, W. H., S. A. Teukolsky, W. T. Vetterling, and B. P. Flannery (1992), *Numerical Recipes*, 2nd ed., 963 pp., Cambridge Univ. Press, Cambridge, U. K.

Qafoku, N. P., J. M. Zachara, C. Liu, P. L. Gassman, O. Qafoku, and S. C. Smith (2005), Kinetic desorption and sorption of U(VI) during reactive transport in a contaminated Hanford sediment, *Environ. Sci. Technol.*, *39*, 3157–3165.

Sawatsky, N., Y. Feng, and M. J. Dudas (1997), Diffusion of l-naphthol and naphthalene through clay materials: Measurement of apparent exclusion of solute from the pore space, *J. Contam. Hydrol.*, *27*, 25–41.

Steefel, C. I. (Ed.) (2007), *Geochemical Kinetics and Transport*, pp. 545–589, Springer, N. Y.

Steefel, C. I., and P. C. Litchner (1994), Diffusion and reaction in rock matrix bordering a hyperalkaline fluid-filled fracture, *Geochim. Cosmochim. Acta*, *58*, 3595–3612.

Steefel, C. I., and K. Maher (2009), Fluid-rock interaction: A reactive transport approach, *Rev. Mineral. Geochem.*, *70*, 485–532, doi:410.2138/rmg.2009.2170.2111.

Stubbs, J. E., L. A. Veblen, D. Elbert, J. M. Zachara, J. A. Davis, and D. R. Veblen (2009), Newly recognized hosts for uranium in the Hanford Site vadose zone, *Geochim. Cosmochim. Acta*, *73*, 1563–1576.

Sukop, M. C., and D. T. J. Thorne (2005), *Lattice Boltzmann Modeling*, 172 pp., Springer, N. Y.

Tartakovsky, A. M., P. Meakin, T. D. Scheibe, and B. D. Wood (2007), A smoothed particle hydrodynamics model for reactive transport and precipitation in porous and fracture porous media, *Water Resour. Res.*, *43*, W05437, doi:10.1029/2005WR004770.

Tokunaga, T. K., J. Wan, M. K. Firestone, T. C. Hazen, E. Schwartz, S. R. Sutton, and M. G. Newville (2001), Chromium diffusion and reduction in soil aggregates, *Environ. Sci. Technol.*, *35*, 3169–3174.

Tokunaga, T. K., J. M. Wan, J. Pena, S. R. Sutton, and M. Newville (2004), Hexavalent uranium diffusion into soils from concentrated acidic and alkaline solutions, *Environ. Sci. Technol.*, *38*, 3056–3062.

Van Cappellen, P., and J.-F. Gaillard (1996), Biogeochemical dynamics in aquatic sediments, *Rev. Mineral.*, *34*, 335–376.

Wang, Z., J. M. Zachara, W. Yantansee, P. L. Gassman, C. Liu, and A. G. Joly (2004), Cryogenic laser induced fluorescence characterization of U(VI) in Hanford vadose zone pore waters, *Environ. Sci. Technol.*, *38*, 5591–5597.

Werth, C. J., J. A. Cunningham, P. V. Roberts, and M. Reinhard (1997), Effects of grain-scale mass transfer on the transport of volatile organics through sediments 2. Column results, *Water Resour. Res.*, *33*, 2727–2740.

Wood, W. W., T. F. Kraemer, and P. P. Hearn (1990), Intragranular diffusion: An important mechanism influencing solute transport in clastic aquifer, *Science*, *247*, 1569–1572.

Yamaguchi, T., and S. Nakayama (1998), Diffusivity of U, Pu, and Am carbonate complexes in a granite from Inada, Ibaraki, Japan studied by through diffusion, *J. Contam. Hydrol.*, *35*, 55–65.

Yamaguchi, T., Y. Sakamoto, S. Nakayama, and T. T. Vandergaaf (1997), Effective diffusivity of the uranyl ion in a granite from Inada, Ibaraki, Japan, *J. Contam. Hydrol.*, *26*, 109–117.

Zheng, Q., and G.-W. Wei (2011), Poisson-Boltzmann-Nernst-Planck model, *J. Chem. Phys.*, *134*, 194101.

C. Liu, J. Shang, and J. M. Zachara, Chemical and Material Science Division, Fundamental and Computational Science Directorate, Pacific Northwest National Laboratory, P.O. Box 999, MSIN K8–96, Richland, WA, 99354, USA. (chongxuan.liu@pnl.gov)